Phenanthrenequinone-Based Hypercrosslinked Polymers via a Waste-Minimizing Friedel-Crafts Alkylation

Manying Liu[a,*], Pan Liu[a], Zikang Lei[b], Rongjuan Ba[a], Suxiang Ge[a], Jiachang Li[a], Huimin Jia[a], Yuanting Qiao[c], Yange Zhang[a,*], and Zhi Zheng[a]

[a]Key Laboratory of Micro-Nano Materials for Energy Storage and Conversion of Henan Province, Institute of Surface Micro and Nano Materials, College of Chemical and Materials Engineering, Xuchang University, Henan 461000, China

E-mail addresses: manyingliu988@xcu.edu.cn (M. Liu), zhangyg@xcu.edu.cn (Y. Zhang)

[b]College of Chemistry, Zhengzhou University, Zhengzhou 450001, China

[c]Chemical Engineering Department, Swansea University, Bay Campus, Swansea, SA1 8EN, UK.

ABSTRACT: Although hypercrosslinked polymers (HCPs) offer significant advantages, their industrial scalability has been impeded by concerns regarding waste generation. To mitigate this challenge, we have successfully developed an efficient and cost-effective green synthesis method for phenanthrenequinone-based HCPs (PQ-HCPs). This method employs a Friedel-Crafts alkylation reaction, utilizing trifluoromethanesulfonic acid as a catalyst and PQ as the starting material. Under low catalyst concentrations, electrophilic sulfonation reactions are predominant. However, increasing the catalyst to a 2 equivalent amount significantly shifts the reaction pathway towards Friedel-Crafts alkylation cross-linking. The resultant optimal sample,

PQ-HCP-1:3, boasts an impressive specific surface area of up to 428 m^2/g. Dye adsorption experiments on these samples demonstrated a marked selective affinity for Rhodamine B (RB), with the hydrophilicity of the samples being a pivotal factor in the adsorption process. This innovative approach substantially outperforms traditional methods, which typically involve ferric chloride and aluminum chloride, by significantly reducing the production of solid waste and effluent during the chemical reaction process.

KEYWORDS: Hypercrosslinked polymer; Green synthesis; Solid waste; Phenanthrenequinone; Trifluoromethanesulfonic acid

1. INTRODUCTION

The growing need for sustainable technologies drives the importance of green synthesis, which is essential for advancing the development of porous organic polymers (POPs) with their potential benefits [1, 2]. POPs include covalent organic frameworks (COFs) [3-6], hypercrosslinked porous polymers (HCPs) [7-10], conjugated microporous polymers (CMPs) [11-13], polymers of intrinsic microporosity (PIMs) [14-16], covalent triazine frameworks (CTFs)[17-21], and porous aromatic frameworks (PAFs) [22, 23]. Among these, HCPs stand out due to their unique synthesis through the Friedel-Crafts alkylation reaction [7, 24, 25]. Importantly, HCPs are recognized for their low synthesis costs, making them economically valuable and industrially viable materials. This economic viability is largely attributed to the use of low-cost raw materials—including monomers, reaction media, and catalysts—as well as manageable reaction conditions that yield high product outputs [25]. Owing to these advantageous characteristics, HCPs are promising

candidates for a wide range of applications, including gas storage[10, 26], carbon capture[25, 27], pollutant removal[28, 29], microwave adsorption[30], and catalysis[31].

However, the industrialization of HCPs has been challenged by significant environmental concerns, particularly the pollution caused by solid waste generated during their synthesis process. The synthesis of HCPs primarily occurs through three approaches: (1) post-crosslinking of polymer precursors[32], (2) direct one-step polycondensation of functional monomers[33, 34], and (3) interweaving rigid aromatic building blocks with external crosslinkers[35, 36]. Despite these methods, the process often requires substantial amounts of heterogeneous catalysts, such as ferric chloride and aluminum chloride[37]. The separation of solid HCPs from catalyst residues is complicated, and recycling these residues poses additional difficulties. Furthermore, the washing of these residues contributes to significant liquid waste, resulting in high economic costs and severe environmental pollution, which further hinders the industrial production of HCPs[38].

To address these pressing challenges, there is a critical need for the development of more sustainable and efficient synthetic methods. Innovations in catalyst design, such as employing homogeneous catalysts that can be easily separated and recycled, or exploring alternative, greener synthetic pathways, could facilitate broader industrial applications of HCPs while mitigating their environmental impact. Additionally, it is worth noting that, to our knowledge, the synthesis of hypercrosslinked polymers based on phenanthrenequinone has not yet been successfully achieved due to the electron-deficient nature of the quinone functional group, indicating further opportunities for research and development in this area.

In this work, we developed an eco-friendly synthesis method for phenanthrenequinone-based hypercrosslinked polymers (PQ-HPs) using Friedel-Crafts alkylation with trifluoromethanesulfonic acid as the catalyst. By replacing harmful ferric chloride and aluminum chloride catalysts, our innovative method minimizes waste generation and promotes a more sustainable chemical process. The optimal synthesis ratio of phenanthrenequinone to catalyst was found to be 1:3, yielding the product with the maximum specific surface area. The PQ-HCPs display superior adsorption capabilities for Rhodamine B (RB) dye, particularly in acidic conditions, due to their super-hydrophilic properties. They also showed excellent recyclability.

2. EXPERIMENTAL METHODS

2.1 Synthetic procedures of PQ-HCPs

To synthesize PQ-HCP samples, a mixture of phenanthrenequinone (PQ), dimethoxymethane (FDA), and 1, 2-Dichloroethane (DCE) is first prepared in a molar ratio of 1:4:4 and added to a round-bottom flask. Trifluoromethanesulfonic acid is then added dropwise in equivalent ratios of 1, 1.5, 2, 3, or 4. The mixture is stirred in an ice bath for 2 hours to ensure thorough mixing. Following this, the reaction system is heated to 40°C maintained at this temperature for 4 hours to facilitate the reaction. To further enhance the reaction, the temperature is increased to 80°C, and the mixture is heated and stirred for an additional 4 hours. The reaction is then quenched with anhydrous ethyl alcohol, followed by filtration to separate the solid product from the liquid phase. The solid product is washed with deionized water for

an additional 2 hours to remove any remaining solvents and impurities. Finally, vacuum freeze-drying is employed for 8 hours to obtain the dry PQ-HCP sample powder.

2.2 Investigation of adsorption performance of PQ-HCPs

The adsorption capacity of PQ-HCPs for three specific dyes: To investigate the adsorption capacity of PQ-HCP samples, we prepared 500 mL solutions of Rhodamine B (RB), Methylene Blue (MB), and Methyl Orange (MO), each at a concentration of 20 $mg \cdot L^{-1}$. 100 mL portions from each solution were used for adsorption experiments. To each portion, 0.03 g of PQ-HCP samples was added. We analyzed the adsorption efficiency and dynamics of PQ-HCPs for these dyes by collecting solution samples at various time points and measuring their absorbance with a UV-Vis spectrophotometer. By comparing the changes in absorbance over time, we were able to evaluate the adsorption performance of PQ-HCPs for the target pollutants.

The effect of adsorbent dosage: Initially, a 500 mL solution of Rhodamine B with a concentration of 20 $mg \cdot L^{-1}$ was prepared. Subsequently, 100 mL of this solution was divided into four 250 mL beakers. To each beaker, 0.01 g, 0.03 g, 0.06 g, and 0.10 g of PQ-HCP samples were added to study the adsorption efficiency at different adsorbent dosages. Solution samples were collected at different time points and analyzed using a UV-Vis spectrophotometer to determine the adsorption effect.

The effect of pH: A 500 mL solution of Rhodamine B at a concentration of 20 $mg \cdot L^{-1}$ was prepared and divided into 100 mL portions in seven beakers for the adsorption experiment. The pH values of the solutions in the beakers were adjusted to 2, 4, 6, 8, 10, and 12 using dilute HCl and NaOH solutions, respectively. Into each beaker, 0.0300 g of PQ-HCP samples were

added, albeit with slight variations in actual weighing (0.0301 g, 0.0307 g, 0.0301 g, 0.0301 g, 0.0304 g, 0.0300 g). Solution samples were collected at different time points and analyzed using a UV-Vis spectrophotometer.

The reusability of PQ-HCP samples: The reusability of PQ-HCP samples was explored. The used PQ-HCP samples were treated with ethanol to elute the adsorbed Rhodamine B dye from the sample surface, continuing until the eluent reached a colorless state, indicating complete removal of Rhodamine B. Thereafter, the eluted PQ-HCP samples were subjected to vacuum freeze-drying to ensure sample dryness and reusability. The dried PQ-HCP samples were then reused in the adsorption experiment under the same conditions as before, repeated three times, to test the adsorption performance and cyclic stability of PQ-HCPs. In each adsorption experiment, solution samples were collected at different time points and subsequently analyzed using a UV-Vis spectrophotometer.

3. RESULTS AND DISCUSSION

The PQ-HCP samples were synthesized using a Friedel-Crafts alkylation reaction, with trifluoromethanesulfonic acid as the catalyst and PQ as the raw material (Figure 1). The molar ratio of PQ to catalyst was modified from 1:1 to 1:4. The samples are denoted based on the PQ to catalyst ratio: PQ-HCP-1:1 for a ratio of 1:1, PQ-HCP-1:1.5 for a ratio of 1:1.5, PQ-HCP-1:2 for a ratio of 1:2, PQ-HCP-1:3 for a ratio of 1:3, and PQ-HCP-1:4 for a ratio of 1:4, respectively. Fourier-transform infrared (FT-IR) spectroscopy was employed to elucidate the structure of the PQ-HCP samples. As shown in Figure 2a, PQ-HCP-1:3 exhibits new

characteristic peaks after cross-linking, distinct from the PQ raw material. Specifically, the FT-IR spectra reveal symmetric (2921 cm^{-1}) and asymmetric (2846 cm^{-1}) stretching vibrations of the methylene group (-CH_2-), as well as a peak at 1384 cm^{-1} corresponding to its bending vibration[8, 39]. This indicates that the cross-linked product (PQ-HCP-1:3) formed after the reaction between the FDA and PQ contains a -CH_2- group. From Figure 2b, we identified several key absorption peaks: the peaks at 1601 cm^{-1}, 1502 cm^{-1}, and 1450 cm^{-1} are all related to the vibrational absorption of the benzene ring framework. The presence of these peaks confirms the integrity of the benzene ring structure in the sample. Additionally, the absorption peak at 1676 cm^{-1} is attributed to the C=O stretching vibration, characteristic of the quinone functional group in PQ. The observation of these characteristic peaks indicates that a successful cross-linking reaction has occurred between PQ and FDA, and during this process, the basic unit structure of PQ has been effectively preserved.

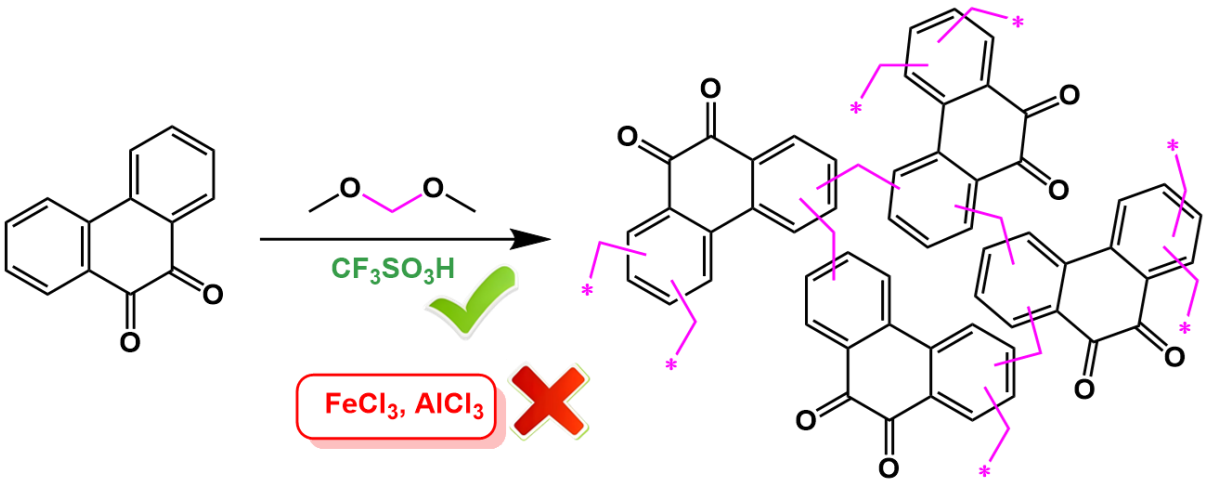

Figure 1. The synthesis process of phenanthrenequinone-based hypercrosslinked polymers (PQ-HCPs).

To further elucidate the structure of the PQ-HCP-1:3 product, solid-state cross-polarization magic angle spinning ^{13}C nuclear magnetic resonance (CP-MAS ^{13}C-NMR) spectroscopy was employed. The CP-MAS ^{13}C-NMR spectrum (Figure 2c) reveals signals at 185 ppm, which are characteristic of the quinonyl carbon. Signals in the range of 120-145 ppm correspond to the phenyl carbons of PQ-HCP-1:3[40]. Additionally, two distinct resonances at approximately 35 ppm and 30 ppm are observed, which are attributed to the carbon atoms of -CH_2- groups formed after cross-linking[8]. The splitting of these signals into two peaks is indicative of the differing chemical environments of the methylene groups attached to the benzene ring, a variation that is typical of the unpredictable substitution sites in the Friedel-Crafts reaction, an electrophilic aromatic substitution process. The peak at 65 ppm is attributed to the carbon resonance in the solvent dichloroethane. Chemical characterization results indicate that a cross-linked network was formed between FDA and PQ through Friedel-Crafts alkylation. In this process, FDA acted as an external cross-linking agent, facilitating the connection between PQ molecules and constructing a stable network structure. This structure not only enhances the overall performance of the material but may also significantly affect its chemical and physical properties.

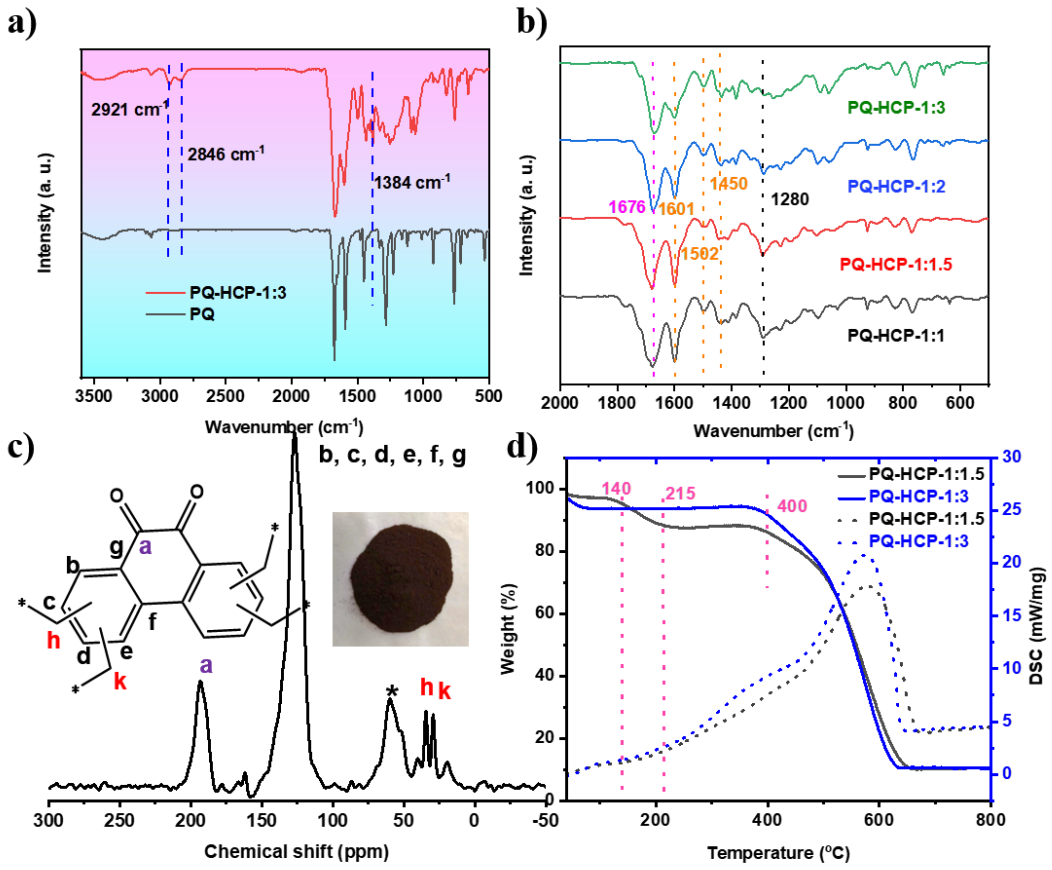

Figure 2. (a) FT-IR spectra of PQ-HCP-1:3 and PQ samples; (b) The local FT-IR spectra of PQ-HCPs; (c) CP-MAS ^{13}C-NMR spectrum of PQ-HCP-1:3; Inset: The digital image of the PQ-HCP-1:3 sample; (d) TGA and DSC thermograph of PQ-HCP-1:1.5 and PQ-HCP-1:3.

Thermogravimetric analysis (TGA) and differential scanning calorimetry (DSC) conducted under a nitrogen atmosphere (Figure 2d) revealed that the PQ-HCP-1:3 and PQ-HCP-1:1.5 samples began to decompose at 400°C, with complete decomposition at 632°C, indicating their excellent thermal stability at elevated temperatures. The DSC curve exhibited a notable increase in the exothermic reaction rate around 400°C, peaking at 578°C, which further corroborates this observation. Notably, the PQ-HCP-1:1.5 sample started to decompose at 140°C and was fully decomposed by 215°C, whereas the PQ-HCP-1:3 sample did not show this behavior at lower temperatures, possibly due to the decomposition characteristics of the

sulfonic acid groups. In the FT-IR spectral analysis, an absorption peak at approximately 1280 cm^{-1} was observed, corresponding to the stretching vibration of S=O (Figure 2b)[41]. This suggests that a partial sulfonation reaction may have occurred during the reaction process. Contact angle testing provided insights into the hydrophilicity of the PQ-HCPs materials, with images of water droplet contact angles shown in Figure S1. The measured contact angles were as follows: 37.1° for Figure S1a, 6.7° for Figure S1b, 67.5° for Figure S1c, and 68.7° for Figure S1d. Based on these measurements, the hydrophilicity of the four types of PQ-HCPs samples, from highest to lowest, is PQ-HCP-1:1.5, PQ-HCP-1:1, PQ-HCP-1:2, and PQ-HCP-1:3[42]. Further analysis revealed that when the amount of trifluoromethanesulfonic acid catalyst is low, sulfonation is the predominant reaction; however, when the catalyst amount reaches 2 equivalents, the cross-linking reaction becomes the primary process. For the synthesis of porous materials, the Brunauer−Emmett−Teller (BET) surface area and pore size distribution are closely related to the design of the cross-linking process.

Nitrogen gas adsorption isotherms of PQ-HCPs at 77 K show a transition from type III to type II as the amount of trifluoromethanesulfonic acid increases (Figure 3a), indicating an increase in micropore presence. This suggests that at lower catalyst concentrations, sulfonation is the dominant process, leading primarily to the formation of macropores through layer stacking. When the catalyst reaches a 2-equivalent concentration, the reaction shifts towards Friedel-Crafts cross-linking, resulting in micropore formation. The surface area of PQ-HCPs was calculated using the BET model, and the pore size distribution was analyzed using nonlocal density functional theory. With less than 2 equivalents of catalyst, the specific surface area

peaks at only 95 m^2/g, and the pore volume capacity reaches a maximum of 0.2616 cm^3/g (Table 1). Notably, the yield exceeds 100%, reaching 112%. The pore size distribution graph confirms a predominance of macropores (Figure 3b), supporting the notion that sulfonation is the primary reaction with smaller catalyst amounts. At 3 equivalents of catalyst, the specific surface area of PQ-HCPs increases to 428 m^2/g, with a yield of 88% and a pore size distribution ranging from 0.4 nm to 3.4 nm.

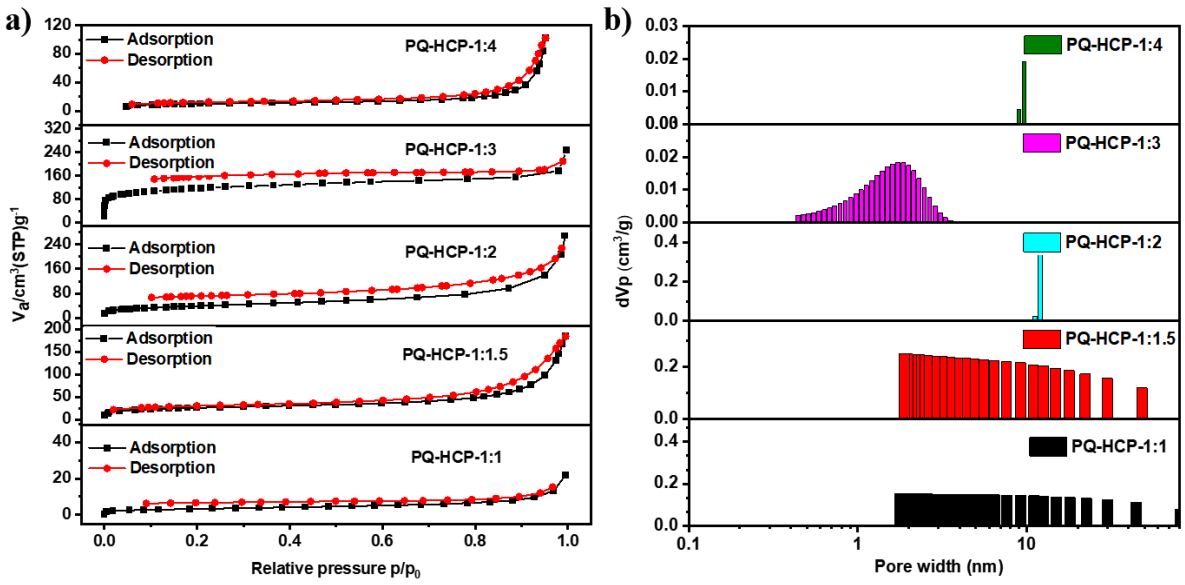

Figure 3. (a) Nitrogen gas adsorption isotherms for PQ-HCPs at 77 K; (b) Pore size distributions of PQ-HCPs.

However, an excessive amount of catalyst seems to disrupt the Friedel-Crafts alkylation cross-linking reaction, leading to a decrease in specific surface area. This innovative green synthesis approach for PQ-HCPs leverages the Friedel-Crafts reaction such that, with a lower catalyst amount, it primarily facilitates sulfonation. Once the catalyst reaches an optimal level, it overcomes the reaction's energy barrier, enabling cross-linking to proceed. Yet, an excess of catalyst can counterproductively hinder the Friedel-Crafts process, underscoring the critical

role of catalyst concentration in achieving desired material properties. This method demonstrates the crucial role of carefully balancing catalyst usage in achieving desired porosity and surface properties for PQ-HCP synthesis.

Table 1. Yields, specific surface areas (SSA_{BET}), and pore volume of PQ-HCPs

Polymer	PQ: TfOH	Yield (%)	SSA_{BET} /($m^2 \cdot g^{-1}$)	V_{total}/($cm^3 \cdot g^{-1}$)
PQ-HCP-1:1	1: 1	101%	37	0.1404
PQ-HCP-1:1.5	1: 1.5	112%	95	0.2616
PQ-HCP-1:2	1: 2	99%	148	0.3604
PQ-HCP-1:3	1: 3	88%	428	0.3375
PQ-HCP-1:4	1: 4	86%	85	0.0311

The brownish-red sample PQ-HCP-1:3, which has the highest specific surface area as indicated in the inset of Figure 2c, was selected for X-ray powder diffraction (XRD) analysis. A broad diffraction peak was observed around $2\theta = 22°$, which is typically attributed to the interaction of π-electron clouds in aromatic structures, known as the π-π stacking effect (see Figure S2). The presence of this broad peak indicates a disordered molecular arrangement in the PQ-HCP-1:3 sample, confirming its amorphous nature. Elemental analysis for PQ-HCP-1:3 revealed a composition of carbon (C) at 72.47%, hydrogen (H) at 5.054%, sulfur (S) at 2.325%, and oxygen(O) at 19.67% (Table S1). The scanning electron microscopy (SEM) characterization of PQ-HCPs is presented in Figure 4, where Figures 4a to 4d correspond to PQ-HCP-1:1, PQ-HCP-1:1.5, PQ-HCP-1:2, and PQ-HCP-1:3, respectively. As observed from the images, PQ-HCPs display a stacked spherical morphology. With an increase in the amount

of trifluoromethanesulfonic acid, the particle size of PQ-HCPs becomes progressively more uniform, finer, and fluffier. The unique structure of these porous polymers, combined with their quinone groups, makes them ideal candidates for efficient dye removal in wastewater treatment processes.

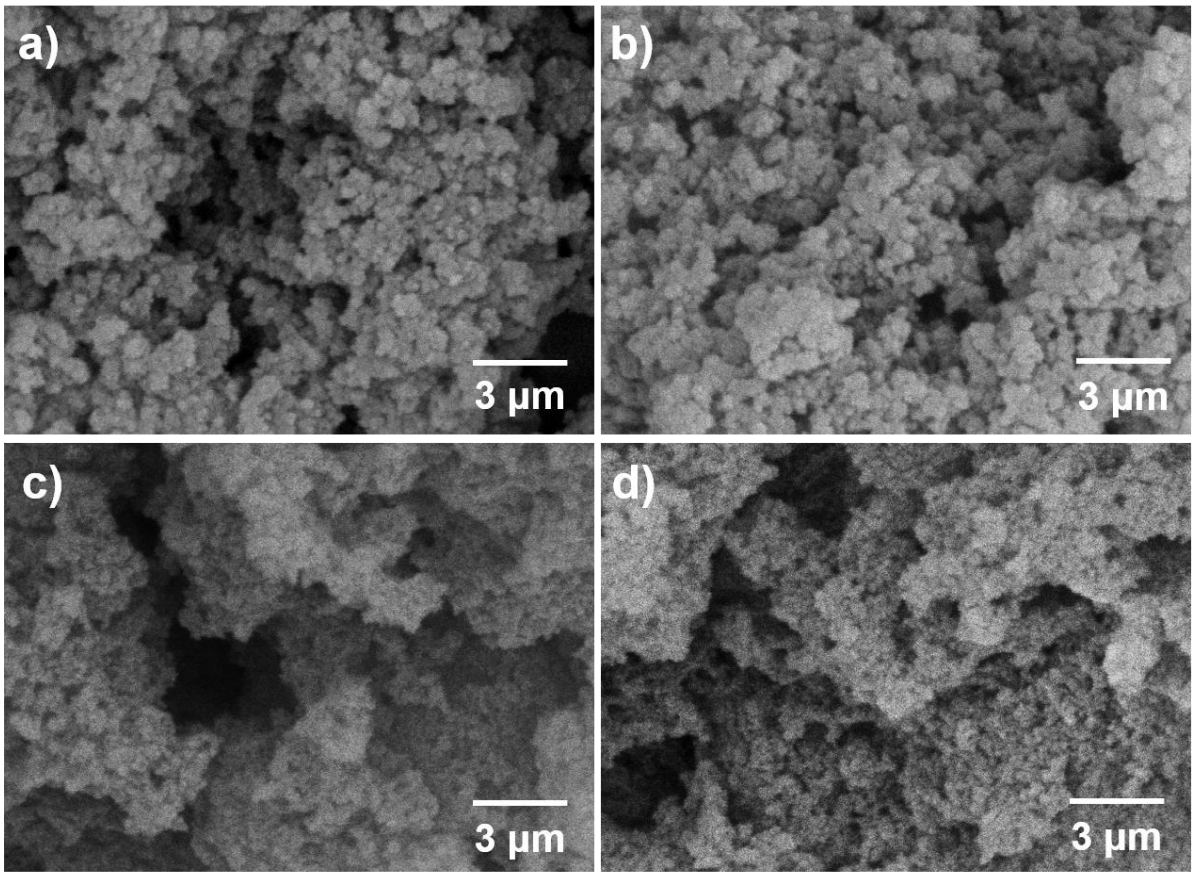

Figure 4. SEM images of (a) PQ-HCP-1:1, (b) PQ-HCP-1:1.5, (c) PQ-HCP-1:2, (d) PQ-HCP-1:3.

To evaluate the adsorption efficacy of PQ-HCP-1:1, PQ-HCP-1:1.5, PQ-HCP-1:2, and PQ-HCP-1:3 on RB, adsorption solutions were collected at regular intervals for analysis and subsequently plotted the adsorption kinetics (Figure 5a). The experimental results indicate that the PQ-HCP-1:1 sample achieved an RB removal rate of 80.33%. In contrast, the PQ-HCP-

1:1.5 sample demonstrated the highest removal rate at 96.07%. The PQ-HCP-1:2 sample had a removal rate of 95.18%, while the PQ-HCP-1:3 sample showed a reduced removal rate of 75.56% (Figure 5b). This variation is likely attributed to the superhydrophilic nature of PQ-HCP-1:1.5, which enhances its interaction with RB molecules, resulting in the most pronounced adsorption effect. Furthermore, the adsorption effect of PQ-HCPs on RB solution is significantly influenced by the amount used. Experimental data indicate that when the dosages of PQ-HCP-1:1.5 were 0.01 g, 0.03 g, 0.06 g, and 0.10 g, the corresponding removal rates of RB were 55.56%, 94.59%, 97.29%, and 99.47%, respectively (Figure 5c and Figure S3). Calculations reveal that using PQ-HCPs as an adsorbent achieved an adsorption capacity of 188 mg/g for RB. Thus, increasing the adsorbent dosage enhances the adsorption efficiency within the same time frame.

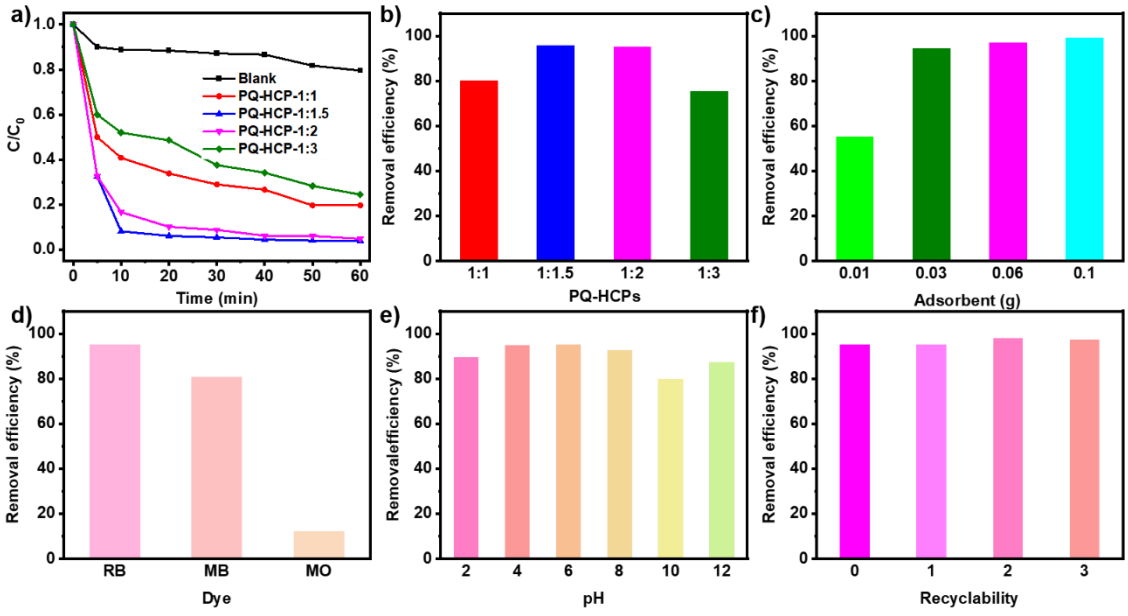

Figure 5. (a) Adsorption kinetics of PQ-HCPs plotted as adsorption ratio (adsorbed amount/ total amount) versus time; (b) The removal efficiency of RB by PQ-HCPs; (c) The impact of

different amounts of PQ-HCP-1:1.5 on the removal efficiency of RB; (d) Removal efficiencies of various dyes; (e) The effect of pH values on the removal efficiency of RB; (f) Recyclability of removal RB with PQ-HCP-1:1.5.

Due to the presence of lone pairs of electrons from the two carbonyl groups in PQ-HCPs, an electrostatic adsorption mechanism is likely at play. This could result in different adsorption performances for cationic dyes such as RB and Methylene Blue (MB), as well as the anionic dye Methyl Orange (MO). To investigate the selective adsorption properties of PQ-HCPs, solutions of RB, MB, and MO were prepared at identical concentrations and subjected to adsorption using equal amounts of PQ-HCPs. As illustrated in Figure 5d and Figure S4, PQ-HCPs exhibit significant adsorption effects on both RB and MB. Notably, the adsorption of the cationic dye RB by PQ-HCPs is more effective than that of the anionic dye MO. This phenomenon is likely due to better charge matching between PQ-HCPs and the positively charged dye molecules, which facilitates the adsorption process[29].

To further elucidate the adsorption mechanism, the Freundlich, Langmuir, and Tempkin adsorption isotherm models were employed to investigate the thermal effects of dye adsorption on polymers. The maximum adsorption capacities (qe) of 20 mg of PQ-HCP-1:1.5 on 50 mL of RB solutions with concentrations of 50, 100, 150, 180, 200, and 250 mg/L after 30 minutes of adsorption at 298 K are depicted in Figure S5. The Freundlich, Langmuir, and Tempkin models were fitted to the experimental data, and the adsorption isotherm parameters were obtained as shown in Table S2. From the fitting results, at the same temperature, the overall fit of the models in descending order of accuracy is Tempkin > Langmuir > Freundlich. The

Tempkin model more accurately describes the adsorption process under experimental conditions compared to the other two models. According to the assumptions of the Tempkin isotherm model, which posits that the adsorption heat changes linearly with surface coverage, it can be inferred that there is an electrostatic interaction between PQ-HCP-1:1.5 and RB molecules[43].

To assess the influence of pH on adsorption efficiency, we adjusted the pH of RB solutions across six gradients, from pH 2 to 12 (as shown in Figure 5e), using dilute HCl and NaOH solutions for the adsorption experiments. The data revealed that the removal rates under these varying pH conditions were relatively similar, with a slight enhancement in adsorption efficiency under acidic conditions. To evaluate the recyclability of the adsorbent, we performed adsorption experiments on PQ-HCP-1:1.5, which exhibited the highest removal rate. Initially, the sample achieved a removal rate of 95.18% within one hour. After the first cycle of recovery and reuse (as depicted in Figure 5f), the removal rate was 95.36%. This rate increased to 98.08% after the second cycle and slightly decreased to 97.46% after the third cycle. These results suggest that the adsorption performance remains consistent across multiple reuse cycles, indicating the excellent recyclability of PQ-HCPs. Notably, after several cycles of use, no structural alterations were observed in the samples, as confirmed by FT-IR spectroscopy (Figure S6) and XRD analysis (Figure S7).

4. CONCLUSIONS

In summary, we have developed a green synthesis method for a class of PQ-HCPs by replacing the traditional ferric chloride and aluminum chloride catalysts. The success of this approach

hinges on the precise control of the trifluoromethanesulfonic acid catalyst quantity. At low catalyst concentrations, electrophilic sulfonation reactions predominate, but increasing the catalyst to a 2 equivalent level shifts the reaction mechanism towards Friedel-Crafts alkylation cross-linking. Our optimized synthesis conditions, featuring a molar ratio of 1:3 between phenanthrenequinone and catalyst, yield a product with an impressive specific surface area of 428 m^2/g. The PQ-HCPs showcase exceptional performance owing to their super-hydrophilic nature, which enhances their adsorption capacity for Rhodamine B dye, especially in acidic environments. This green synthetic approach not only offers a new strategy for the large-scale, cost-effective production of HCPs but also eliminates solid waste generation, aligning with the principles of sustainable chemistry.

ASSOCIATED CONTENT

The Supporting Information is available free of charge at xxx.

Materials and characterization. Contact angle testing of PQ-HCPs. XRD patterns of PQ-HCP-1:3. Adsorption kinetics of PQ-HCPs for RB, MB, and MO. UV-vis absorption spectra of PQ-HCP-1:1.5 with varying amounts. FT-IR spectra. Elemental analysis.

AUTHOR INFORMATION

Corresponding authors

Manying Liu − *Key Laboratory of Micro-Nano Materials for Energy Storage and Conversion of Henan Province, Institute of Surface Micro and Nano Materials, College of Chemical and Materials Engineering, Xuchang University, Henan 461000, China*

ORCID: https://orcid.org/0000-0002-7849-7980

E-mail: manyingliu988@xcu.edu.cn

Yange Zhang − *Key Laboratory of Micro-Nano Materials for Energy Storage and Conversion of Henan Province, Institute of Surface Micro and Nano Materials, College of Chemical and Materials Engineering, Xuchang University, Henan 461000, China*

ORCID: https://orcid.org/0000-0003-1795-1673

E-mail: zhangyg@xcu.edu.cn

Authors

Pan Liu − *Key Laboratory of Micro-Nano Materials for Energy Storage and Conversion of Henan Province, Institute of Surface Micro and Nano Materials, College of Chemical and Materials Engineering, Xuchang University, Henan 461000, China*

Rongjuan Ba− *Key Laboratory of Micro-Nano Materials for Energy Storage and Conversion of Henan Province, Institute of Surface Micro and Nano Materials, College of Chemical and Materials Engineering, Xuchang University, Henan 461000, China*

Zikang Lei − *College of Chemistry, Zhengzhou University, Zhengzhou 450001, China*

Suxiang Ge − *Key Laboratory of Micro-Nano Materials for Energy Storage and Conversion of Henan Province, Institute of Surface Micro and Nano Materials, College of Chemical and Materials Engineering, Xuchang University, Henan 461000, China*

Jiachang Li − *Key Laboratory of Micro-Nano Materials for Energy Storage and Conversion of Henan Province, Institute of Surface Micro and Nano Materials, College of Chemical and Materials Engineering, Xuchang University, Henan 461000, China*

Huimin Jia − *Key Laboratory of Micro-Nano Materials for Energy Storage and Conversion of Henan Province, Institute of Surface Micro and Nano Materials, College of Chemical and Materials Engineering, Xuchang University, Henan 461000, China*

Yuanting Qiao − *Chemical Engineering Department, Swansea University, Bay Campus, Swansea, SA1 8EN, UK.*

Zhi Zheng − *Key Laboratory of Micro-Nano Materials for Energy Storage and Conversion of Henan Province, Institute of Surface Micro and Nano Materials, College of Chemical and Materials Engineering, Xuchang University, Henan 461000, China*

ORCID: https://orcid.org/0000-0002-5889-4305

Notes

The authors declare no competing financial interest.

ACKNOWLEDGMENT

This work was financially supported by National Natural Science Foundation of China (Grant No. 52072327, 62274141, 22276160); Higher Education and Teaching Reformation Project (2024SJGLX0451); Academic Degrees & Graduate Education Reform Project of Henan Province (YJS2022JD34); Key Research and Development Projects of Universities in Henan Province (23B430009); Natural Science Foundation of Henan Province (232300420099).

REFERENCES

(1) Jiang, S.; Li, Z.; Yang, X.; Li, M.; Wang, C.; Wang, Z.; Wu, Q. Sustainable and Green Synthesis of Porous Organic Polymer for Solid-Phase Extraction of Four Chlorophenols in Water and Honey. *Food Chem.* **2023**, *404*, 134652.

(2) Luo, D.; Shi, T.; Li, Q. H.; Xu, Q.; Strømme, M.; Zhang, Q. F.; Xu, C. Green, General and Low‐Cost Synthesis of Porous Organic Polymers in Sub‐Kilogram Scale for Catalysis and Co2 Capture. *Angew. Chem. Int. Ed.* **2023**, *62* (27), e202305225.

(3) Zhu, Y.; Huang, D.; Wang, W.; Liu, G.; Ding, C.; Xiang, Y. Sequential Oxidation/Cyclization of Readily Available Imine Linkages to Access Benzoxazole‐Linked Covalent Organic Frameworks. *Angew. Chem. Int. Ed.* **2024**, *63* (11), e202319909.

(4) Tao, S.; Jiang, D. Exceptional Anhydrous Proton Conduction in Covalent Organic Frameworks. *J. Am. Chem. Soc.* **2024**, *146* (26), 18151-18160.

(5) Zhou, Z.; Xiong, X.-h.; Zhang, L.; Li, Y.; Yang, Y.; Dong, X.; Lou, D.; Wei, Z.; Liu, W.; Su, C.-y.; et al. Linker-Guided Growth of Single-Crystal Covalent Organic Frameworks. *J. Am. Chem. Soc.* **2024**, *146*, 3449-3457.

(6) Liu, Y.; Liu, X.; Su, A.; Gong, C.; Chen, S.; Xia, L.; Zhang, C.; Tao, X.; Li, Y.; Li, Y.; et al. Revolutionizing the Structural Design and Determination of Covalent–Organic Frameworks: Principles, Methods, and Techniques. *Chem. Soc. Rev.* **2024**, *53* (1), 502-544.

(7) Tan, L.; Tan, B. Hypercrosslinked Porous Polymer Materials: Design, Synthesis, and Applications. *Chem. Soc. Rev.* **2017**, *46* (11), 3322-3356.

(8) Yang, S.; Zhong, Z.; Hu, J.; Wang, X.; Tan, B. Dibromomethane Knitted Highly Porous Hyper‐Cross‐Linked Polymers for Efficient High‐Pressure Methane Storage. *Adv. Mater.* **2024**, *36* (19), 2307579.

(9) Wang, L.; Zhang, G.; Zhao, H.; Wang, G.; Li, Z.; Li, C. Phosphorus Coordinated Pd Single-Atom Sites on Hypercrosslinked Polymers for Heterogeneous Hydroesterification of Ethylene. *Chem. Eng. J.* **2024**, *496* (9), 149580.

(10) Su, P.; Chen, S.; Yang, Z.; Zhong, N.; Jiang, C.; Li, W. Vapor-Phase Postsynthetic Amination of Hypercrosslinked Polymers for Efficient Iodine Capture. *Chin. Chem. Lett.* **2024**, *35* (9), 109357.

(11) Peng, Y. Z.; Guo, G. C.; Guo, S.; Kong, L. H.; Lu, T. B.; Zhang, Z. M. Charge Transfer from Donor to Acceptor in Conjugated Microporous Polymer for Enhanced Photosensitization. *Angew. Chem. Int. Ed.* **2021**, *60* (40), 22062-22069.

(12) Ma, H.; Chen, Y.; Li, X.; Li, B. Advanced Applications and Challenges of Electropolymerized Conjugated Microporous Polymer Films. *Adv. Funct. Mater.* **2021**, *31* (33), 2101861.

(13) Lee, J. M.; Cooper, A. I. Advances in Conjugated Microporous Polymers. *Chem. Rev.* **2020**, *120* (4), 2171-2214.

(14) Wang, A.; Tan, R.; Breakwell, C.; Wei, X.; Fan, Z.; Ye, C.; Malpass-Evans, R.; Liu, T.; Zwijnenburg, M. A.; Jelfs, K. E.; et al. Solution-Processable Redox-Active Polymers of Intrinsic Microporosity for Electrochemical Energy Storage. *J. Am. Chem. Soc.* **2022**, *144* (37), 17198-17208.

(15) Yin, H.; Yang, B.; Chua, Y. Z.; Szymoniak, P.; Carta, M.; Malpass-Evans, R.; McKeown, N. B.; Harrison, W. J.; Budd, P. M.; Schick, C.; et al. Effect of Backbone Rigidity on the Glass

Transition of Polymers of Intrinsic Microporosity Probed by Fast Scanning Calorimetry. *ACS Macro Letters* **2019**, *8* (8), 1022-1028.

(16) Du, N.; Dal-Cin, M. M.; Robertson, G. P.; Guiver, M. D. Decarboxylation-Induced Cross-Linking of Polymers of Intrinsic Microporosity (PIMs) for Membrane Gas Separation. *Macromolecules* **2012**, *45* (12), 5134-5139.

(17) Wang, C.; Lyu, P.; Chen, Z.; Xu, Y. Green and Scalable Synthesis of Atomic-Thin Crystalline Two-Dimensional Triazine Polymers with Ultrahigh Photocatalytic Properties. *J. Am. Chem. Soc.* **2023**, *145* (23), 12745-12754.

(18) Guan, L.; Guo, Z.; Zhou, Q.; Zhang, J.; Cheng, C.; Wang, S.; Zhu, X.; Dai, S.; Jin, S. A Highly Proton Conductive Perfluorinated Covalent Triazine Framework Via Low-Temperature Synthesis. *Nat. Commun.* **2023**, *14* (1), 8114.

(19) Zou, Y.; Abednatanzi, S.; Gohari Derakhshandeh, P.; Mazzanti, S.; Schusslbauer, C. M.; Cruz, D.; Van Der Voort, P.; Shi, J. W.; Antonietti, M.; Guldi, D. M.; et al. Red Edge Effect and Chromoselective Photocatalysis with Amorphous Covalent Triazine-Based Frameworks. *Nat. Commun.* **2022**, *13* (1), 2171.

(20) Liu, M.; Huang, Q.; Wang, S.; Li, Z.; Li, B.; Jin, S.; Tan, B. Crystalline Covalent Triazine Frameworks by in Situ Oxidation of Alcohols to Aldehyde Monomers. *Angew. Chem. Int. Ed.* **2018**, *57* (37), 11968-11972.

(21) Huo, L.; Lv, M.; Li, M.; Ni, X.; Guan, J.; Liu, J.; Mei, S.; Yang, Y.; Zhu, M.; Feng, Q.; et al. Amorphous Mno2 Lamellae Encapsulated Covalent Triazine Polymer ‐ Derived Multi ‐

Heteroatoms‐Doped Carbon for ORR/OER Bifunctional Electrocatalysis. *Adv. Mater.* **2024**, *36* (18), 2312868.

(22) Tian, Y.; Zhu, G. Porous Aromatic Frameworks (PAFs). *Chem. Rev.* **2020**, *120* (16), 8934-8986.

(23) Yuan, Y.; Zhu, G. Porous Aromatic Frameworks as a Platform for Multifunctional Applications. *ACS Cent. Sci.* **2019**, *5* (3), 409-418.

(24) Rozyyev, V.; Thirion, D.; Ullah, R.; Lee, J.; Jung, M.; Oh, H.; Atilhan, M.; Yavuz, C. T. High-Capacity Methane Storage in Flexible Alkane-Linked Porous Aromatic Network Polymers. *Nature Energy* **2019**, *4* (7), 604-611.

(25) Wang, S.; Zhang, C.; Shu, Y.; Jiang, S.; Xia, Q.; Chen, L.; Jin, S.; Hussain, I.; Cooper, A. I.; Tan, B. Layered Microporous Polymers by Solvent Knitting Method. *Sci. Adv.* **2017**, *3* (3), e1602610.

(26) Lin, C.; Feng, P.; Wang, D.; Chen, X.; Fang, Y.; Gao, Y.; Zheng, Y.; Yan, Y.; Liu, M. Safe, Facile, and Straightforward Fabrication of Poly(N‐Vinyl Imidazole)/Polyacrylonitrile Nanofiber Modified Separator as Efficient Polysulfide Barrier toward Durable Lithium‐Sulfur Batteries. *Adv. Funct. Mater.* **2024**, 2411872

(27) Wang, S.; Song, K.; Zhang, C.; Shu, Y.; Li, T.; Tan, B. A Novel Metalporphyrin-Based Microporous Organic Polymer with High CO_2 uptake and Efficient Chemical Conversion of CO_2 under Ambient Conditions. *J. Mater. Chem. A* **2017**, *5* (4), 1509-1515.

(28) Peng, Q.; Zhang, Y.-X. Preparation of the 2,2′-Biimidazole-Based Hypercrosslinked Polymers by Bottom-up Synthetic Strategy and Their Application for Adsorping and Fluorescence Sensing 2,4-Dinitrophenol. *J. Solid State Chem.* **2024**, *333*, 124596.

(29) Tang, C.; Hu, T.; Li, Y.; Hu, X.; Song, K. Weaving Hyper‐Crosslinked Polymer from Alkaline Lignin for Adsorption of Organic Dyes from Wastewater. *ChemistrySelect* **2022**, *7* (31), e202200638.

(30) Wang, J.; Wu, F.; Cui, Y.; Chen, J.; Zhang, A.; Zhang, Q.; Zhang, B. Facile Synthesis of Tubular Magnetic Carbon Nanofibers by Hypercrosslinked Polymer Design for Microwave Adsorption. *J. Am. Ceram. Soc.* **2020**, *103* (10), 5706-5720.

(31) Wang, S.; Xu, M.; Peng, T.; Zhang, C.; Li, T.; Hussain, I.; Wang, J.; Tan, B. Porous Hypercrosslinked Polymer-TiO_2-Graphene Composite Photocatalysts for Visible-Light-Driven CO_2 Conversion. *Nat. Commun.* **2019**, *10* (1), 676.

(32) Tsyurupa, M. P.; Blinnikova, Z. K.; Davidovich, Y. A.; Lyubimov, S. E.; Naumkin, A. V.; Davankov, V. A. On the Nature of "Functional Groups" in Non-Functionalized Hypercrosslinked Polystyrenes. *React. Funct. Polym.* **2012**, *72* (12), 973-982.

(33) Wang, K.; Wu, Z.; Tang, L.; Ji, N.; Zhang, C.; Jia, Z.; Liu, M. Synthesis of Extended π‐Conjugated Hypercrosslinked Polymers Via a Friedel–Crafts Reaction and an Intramolecular Scholl Coupling Reaction. *J. Polym. Sci.* **2023**, *62* (8), 1714-1721.

(34) Wang, R.; Wang, X. Y.; Weng, W. J.; Yao, Y.; Kidkhunthod, P.; Wang, C. C.; Hou, Y.; Guo, J. Proton/Electron Donors Enhancing Electrocatalytic Activity of Supported Conjugated Microporous Polymers for CO_2 Reduction. *Angew. Chem. Int. Ed.* **2022**, *61* (5), e202115503.

(35) Woodward, R. T. The Design of Hypercrosslinked Polymers from Benzyl Ether Self-Condensing Compounds and External Crosslinkers. *Chem. Commun.* **2020**, *56* (36), 4938-4941.

(36) Hou, S.; Tan, B. Naphthyl Substitution-Induced Fine Tuning of Porosity and Gas Uptake Capacity in Microporous Hyper-Cross-Linked Amine Polymers. *Macromolecules* **2018**, *51* (8), 2923-2931.

(37) Borrero-López, A. M.; Celzard, A.; Fierro, V. Eco-Friendly Production of Hyper-Cross-Linked Polymers Using Mechanosynthesis and Bioresources: A Critical Review. *ACS Sustain. Chem.Eng.* **2022**, *10* (49), 16090-16112.

(38) Zhu, X.; Ding, S.; Abney, C. W.; Browning, K. L.; Sacci, R. L.; Veith, G. M.; Tian, C.; Dai, S. Superacid-Promoted Synthesis of Highly Porous Hypercrosslinked Polycarbazoles for Efficient Co2 Capture. *Chem. Commun.* **2017**, *53* (54), 7645-7648.

(39) Jia, Z.; Wang, K.; Tan, B.; Gu, Y. Hollow Hyper-Cross-Linked Nanospheres with Acid and Base Sites as Efficient and Water-Stable Catalysts for One-Pot Tandem Reactions. *ACS Catal.* **2017**, *7* (5), 3693-3702.

(40) Wei, R.-R.; Ma, Q.-G.; Sang, Z.-P. Hypolipidemic Phenanthraquinone Derivatives from Heleocharis Dulcis. *Biochem. Syst. Ecol.* **2019**, *83*, 17-21.

(41) Steenackers, M.; Lud, S. Q.; Niedermeier, M.; Bruno, P.; Gruen, D. M.; Feulner, P.; Stutzmann, M.; Garrido, J. A.; Jordan, R. Structured Polymer Grafts on Diamond. *J. Am. Chem. Soc.* **2007**, *129* (50), 15655-15661.

(42) Chen, L.; Gong, Z.; Fu, Z. Study on Organic Fluorine Modified Cationic Acrylic Resin and Its Application in Cathodic Electrodeposition Coatings. *J. Polym. Mater.* **2023**, *40* (3-4), 157-164.

(43) Jang, H. M.; Yoo, S.; Choi, Y.-K.; Park, S.; Kan, E. Adsorption Isotherm, Kinetic Modeling and Mechanism of Tetracycline on Pinus Taeda-Derived Activated Biochar. *Bioresour. Technol.* **2018**, *259*, 24-31.

TOC Image


eliminating solid waste
CF3SO3H
FeCl3, AlCl3
waste generation